

# Atomic-scale Observations of Alloying at the Cr-Fe(001) Interface

A. Davies, Joseph A. Stroscio, D. T. Pierce, and R. J. Celotta

*Electron Physics Group  
National Institute of Standards and Technology  
Gaithersburg, Maryland 20899*

## Abstract

While much progress has been made using epitaxial growth of Fe/Cr/Fe structures to study magnetic exchange coupling, a number of anomalies have arisen in studies of this model system. Using scanning tunneling microscopy and spectroscopy to investigate Cr growth on Fe(001), we have identified a potential structural cause of these anomalies. We show that Cr growth under layer-by-layer conditions on Fe(001) leads to the formation of a Cr-Fe alloy. We exploit a Cr and Fe surface state to identify single Cr impurities in Fe and evaluate the alloy concentrations with increasing Cr coverage.

PACS numbers: 61.16.Ch, 68.55.-a, 75.70.Cn

Significant progress has been made in our understanding of the phenomena of exchange coupling between ferromagnetic layers separated by a non-magnetic layer. In part, this is due to the use of Fe/Cr/Fe as a model system where, under the right conditions, structures produced experimentally can closely approximate those presumed in theoretical calculations [1]. This is advantageous because of the great influence physical structure has on magnetic properties [2] coupled with the general difficulty in growing perfect transition metal structures. High quality Fe/Cr/Fe structures are possible because of the excellent Fe-Cr lattice match (within 0.6%) and the availability of near perfect, single crystal Fe whisker substrates [3]. Such Fe/Cr/Fe structures have revealed more than 70 alignment reversals in the coupling of Fe layers with increasing Cr thickness, allowing the experimental confirmation of the calculated coupling oscillation period to 0.5% accuracy [1].

Recent progress notwithstanding, a number of important anomalies in the magnetic properties of the Cr/Fe and Fe/Cr/Fe systems have arisen, specifically with regard to the change in surface magnetization at low Cr coverages, the antiferromagnetic ordering of the Cr layers, and the size of the Cr moment. Scanning electron microscopy with polarization analysis (SEMPA) measurements of the average magnetization of the topmost surface layers of Cr/Fe(100) show a dramatic decrease during the deposition of the first 0.1 monolayer (ML) of Cr [4]. In recent alternating gradient magnetometer measurements [5] a similar initial rapid decrease in average surface moment is observed, from which it was deduced that the moment of the initially deposited Cr atoms is  $4.5 \mu_B$  [5]. This is more than seven times the bulk moment of  $0.59 \mu_B$ , and even more than the enhanced values of  $3.1 \mu_B$  [6] and  $3.6 \mu_B$  [7] calculated for a Cr surface.

Photoemission measurements of the Cr/Fe(100) interface demonstrate that the first layer of Cr moments align antiparallel to the Fe substrate magnetization [8,9]. With antiferromagnetic stacking of the Cr layers and antiparallel coupling between Cr and Fe, two Fe layers separated by an *odd* number of Cr layers would be expected to align ferromagnetically. In contrast, both SEMPA [1] and Brillouin light scattering (BLS) [10] measurements observe a ferromagnetic alignment between the two Fe layers at *even* Cr layer thickness where oscillatory coupling is observed below 20 monolayers.

In SEMPA measurements of bare Cr on Fe(100), the surface magnetization does not show reversals indicative of antiferromagnetic ordering until the third or fourth layer [1]. Such a delayed onset of clear antiferromagnetic ordering is also observed in inelastic polarized electron scattering measurements, but unlike the SEMPA or BLS measurements, odd layers of Cr are aligned antiparallel to the Fe substrate magnetization [11].

Finally, estimates of the average Cr moment for a monolayer of Cr on Fe(100) from a variety of experiments range from nonexistent [12], to values near that of the bulk [8], to three times the bulk value [13].

Thus, there are conflicting or unexplained results in four areas: indications of a surprisingly high Cr moment for the first  $\sim 0.1$  ML, the unexpected phase of the antiferromagnetic ordering of the Cr layers, the delay in the onset of this ordering, and a lack of consistency in measurements of the average magnetic moment of a Cr monolayer on Fe.

We have investigated a structural cause of these anomalies by carrying out scanning tunneling microscopy (STM) studies of Cr growth on Fe(001). We show that, in contrast to the assumed formation of a chemically abrupt interface, layer-by-layer growth at 300 °C leads

to the formation of a Cr-Fe alloy that is observed as a distribution of single atomic Cr impurities dispersed in the Fe substrate in the submonolayer-coverage regime. In contrast to other STM studies of surface alloys where the source of the image contrast is unknown [14], we use tunneling spectroscopy to identify the density-of-states variations which lead to the atomic-scale chemical contrast. A surface state, seen in conductance spectra on Fe(001) and Cr(001) [15], is used to interpret spectra on the Cr-Fe alloyed surface, leading to a clear chemical identification in the submonolayer Cr coverage regime and an estimate of the chemical composition as the alloy evolves with increasing Cr coverage.

The experiments were performed in an ultra-high vacuum system with facilities for thin film growth and surface characterization by STM and RHEED, as described previously [16]. Cr was deposited at a rate of approximately  $0.8 \text{ ML min}^{-1}$ .

Figure 1(a) shows an image of the surface after depositing 0.4 ML of Cr at a substrate temperature of  $290 \pm 10 \text{ }^\circ\text{C}$  [17]. The layer-by-layer quality of the deposition is clear from the presence of only single atomic-step islands (the uniform lighter grey regions in the image). Because the starting Fe surface is flat on a micron scale [16], the area of the islands provides a calibration of the Cr coverage.

A closer look at the surface reveals small-scale features on both the substrate and island levels as shown in Figure 1 (b). The dark features also appear in STM images of clean Fe whiskers and we believe these are due to contamination from residual gases in the chamber. The small white features on both the substrate and island levels are only seen after depositing Cr. These features are all identical, appearing rotationally symmetric with atomic-scale widths as small as 0.5 nm (FWHM). When imaging the filled (empty) states of the

sample, the features have a maximum apparent positive (negative) height contrast of approximately 0.01 nm. The maximum height contrast of these features compared to the atomic-step islands can be appreciated from the rendered image shown in Figure 1 (c). The height of the atomic-step islands corresponds to the interplanar separation of 0.14 nm for both Cr and Fe along the [001] direction. The size, shape, and voltage-dependence of the dot-like features lead us to identify each feature as a single substitutional impurity atom in the surface layer.

We use tunneling spectroscopy [15] to chemically identify the atoms in the surface alloy by taking advantage of a bcc(001) surface state that lies near the Fermi energy for many transition metals. This surface state leads to a strong and narrow conductance peak at a sample bias of +0.17 V for Fe(001) and -0.05 V for Cr(001), as shown by the dashed curves in Figure 2 [15]. Spectra taken on the Cr-Fe alloyed surface are also shown in the figure (the solid-line curves). When the tip is away from an impurity (over the smooth grey regions in the images) we see a strong conductance peak at the voltage corresponding to the Fe surface state. When the tip is over an impurity atom, the Fe surface state peak is attenuated and a weaker broad peak appears below the Fermi level. The latter conductance peak leads to the positive height contrast of the impurities seen when imaging the filled states of the sample (see Figure 1). These spectral features were reproducibly observed in numerous measurements with different W(111) tips. The two types of spectra are seen on both the exposed regions of the substrate and the islands for submonolayer coverages, indicating that the smooth gray regions in the images are Fe, both on the exposed substrate and island levels, and that the impurity atoms must therefore be Cr. This implies that some of the deposited Cr

atoms have replaced Fe atoms, resulting in a growth layer in the low coverage limit that contains mostly Fe instead of pure Cr (see the schematic in Figure 2).

In the low-coverage regime where the individual Cr atoms can be resolved, the spatial correlation can be evaluated from the Cr-pair distribution function shown in Figure 3 (b). The coordinates of each Cr impurity are determined from the image in Figure 3 (a). The relative position of each Cr pair is found and plotted in Figure 3 (b). Where multiple pairs have the same relative position (within some bin size) the area of the symbol is increased to reflect the number of such pairs. The relative lattice sites corresponding to first, second and third nearest-neighbors [18] are labeled in the figure. Surprisingly, we find no occurrences of first nearest-neighbor Cr pairs. The occupation probability for second nearest neighbors is  $0.038 \pm 0.007$  ML which is only  $0.6 \pm 0.2$  times the value expected for a random distribution ( $0.059 \pm 0.003$  ML). These observations, particularly the absence of first nearest-neighbor Cr pairs, can be appreciated by comparing the impurity features in Figure 3(a) to simulated images of near-neighbor impurities which are shown in the inset. A suppression of nearest-neighbor occupation is indicative of an effective repulsive interaction between the Cr impurities, which is an interesting contrast to many other surface alloys studies where clustering is observed [19].

The variation of the Cr impurity concentration with submonolayer Cr coverage is shown in Figure 4 for growth at 300 °C. The Cr concentrations on the exposed regions of the substrate (islands) are indicated by empty (filled) circles. The Cr concentration on the islands could only be clearly determined for low coverages, and we find no significant difference between the substrate and island concentrations in this limit. The initial slope in

Figure 3 (b) is approximately 0.25, indicating that only one out of every four deposited Cr atoms remains in the surface layers. Beyond a coverage of 0.2 ML, the Cr concentration of islands is difficult to evaluate, but qualitatively appears to increase (see Figure 1 (b)). From ~ 0.2 ML to 1 ML coverages, the Cr accumulation rate in the exposed substrate layer decreases, and consequently the Cr concentration in these regions approaches a constant value of approximately 0.10 ML.

Beyond a Cr coverage of 1 ML, the Cr concentration in the topmost surface layer appears to continue increasing. The images still have an alloyed appearance at coverages of 2-3 ML [20] with all conductance spectra still showing a peak near the Fermi energy. Now, however, the majority of the peak maxima fall at the Cr surface state voltage of  $-0.05$  V, instead of  $-0.3$  V corresponding to the single impurity spectra (see Figure 2), and no peak maxima are observed at the Fe surface state voltage. We therefore infer that the surface is predominantly Cr at these coverages.

To begin to understand the implications of the interfacial alloy on the magnetic properties, we must know the final Cr-Fe concentration profile across the interface. We can only evaluate the surface concentrations from the STM data. By comparing surface concentrations to the Cr deposition, we know that growth at  $300$  °C leads to significant Cr interdiffusion below the surface. Very recent angle-resolved Auger electron spectroscopy experiments on this system show Cr as deep as the third layer below the surface for submonolayer growth at  $\sim 300$  °C [21]. The tunneling spectroscopy measurements suggest the first predominantly-Cr layer occurs at a Cr coverage of no more than 2-3 ML.

A diffuse rather than chemically abrupt Cr/Fe interface could account for many of the

magnetic anomalies in Cr/Fe systems. The phase of the antiferromagnetic ordering of Cr growth on Fe(001) [4] as well as the suppression of clear antiferromagnetic ordering up to the third or fourth layer may result from the spatially varying Cr concentration and the uncertainty in the position of an effective Cr/Fe interface. The large Cr moments deduced from the rapid decrease in the net magnetization in depositing Cr on Fe, as observed in SEMPA [4], and other measurements [5], may be a consequence of the changes in Cr and neighboring Fe moments in the dilute Cr-Fe alloy [22]. Experimental determinations of Cr moments which assume a chemically abrupt interface should be reinterpreted given the Cr-Fe alloying shown here. We believe much of the variation in experimental estimates of the Cr moment in the first Cr layer is due in part to varying degrees of interfacial alloying.

In summary, we have shown that under conditions found best for layer-by-layer growth, Cr growth on Fe(001) leads to the formation of an interfacial Cr-Fe alloy that is observed as single-atom Cr impurities in the substrate and first growth layer. We have identified a spatial correlation among the alloyed Cr atoms that indicates the presence of an effective repulsive interaction. The coverage dependence of the alloy concentration shows that a significant amount of the deposited Cr is below the surface in the submonolayer-coverage regime and that the Cr concentration in the exposed substrate regions saturates at ~10 % of a monolayer as the Cr coverage approaches 1 monolayer.

We would like to thank M. D. Stiles for many helpful discussions and A. Zangwill for the suggestion that interfacial alloying may be operative in the Cr/Fe system. This work was supported in part by the Office of Naval Research.

## References

1. J. Unguris, D. T. Pierce, R. J. Celotta, and J. A. Stroschio, in *Magnetism and Structure in Systems of Reduced Dimension*, edited by R. F. C. Farrow et al. (Plenum, New York, 1993), p. 101; J. Unguris, R. J. Celotta, and D. T. Pierce, Phys. Rev. Lett. **67**, 140 (1991).
2. D. T. Pierce, J. A. Stroschio, J. Unguris, and R. J. Celotta, Phys. Rev. B **49**, 14564 (1994).
3. A. S. Arrott, B. Heinrich, and S. T. Purcell, in *Kinetics of Ordering and Growth at Surfaces*, edited by M. G. Lagally (Plenum, New York, 1990), p. 321.
4. D. T. Pierce, R. J. Celotta, and J. Unguris, J. Appl. Phys. **73**, 6201 (1993); J. Unguris, R. J. Celotta, and D. T. Pierce, Phys. Rev. Lett. **69**, 1125 (1992).
5. C. Turtur and G. Bayreuther, Phys. Rev. Lett. **72**, 1557 (1994).
6. C. L. Fu, A. J. Freeman, and T. Oguchi, Phys. Rev. Lett. **54**, 2700 (1985).
7. R. H. Victora and L. M. Falicov, Phys. Rev. B **31**, 7335 (1985).
8. F. U. Hillebrecht, Ch. Roth, R. Jungblut, E. Kisker, and A. Bringer, Europhys. Lett. **19**, 711 (1992).
9. P. D. Johnson, N. B. Brookes and Y. Chang, MRS Symp. Proc. **231**, 49 (1992).
10. B. Heinrich, Z. Celinski, J.F. Cochran, and M. From, in Proceedings of NATO Advanced Study Institute, Ed. by R.F.C. Farrow, B. Dieny, M. Donath, A. Fert, B.D. Hermsmeir, Series **B309**, 101 (1993).
11. T. G. Walker, A. W. Pang, and H. Hopster, Phys. Rev. Lett. **69**, 1121 (1992).
12. M. Donath, D. Scholl, D. Mauri, and E. Kay, Phys. Rev. B **43**, 13164 (1991).

13. P. Fuchs, K. Totland, and M. Landolt, 14 Inter. Colloq. on Magnetic Films and Surfaces/E-MRS Symposium on Magnetic Ultrathin Films and Multilayers and Surfaces, Dusseldorf, September 1994.
14. See J. L. Stevens and R. Q. Hwang, Phys. Rev. Lett. **74**, 2078 (1995) and references within.
15. J. A. Stroscio, D. T. Pierce, A. Davies, R. J. Celotta, and M. Weinert, Phys. Rev. Lett. **75**, 2960 (1995).
16. J. A. Stroscio, D. T. Pierce, and R. A. Dragoset, Phys. Rev. Lett. **70**, 3615 (1993).
17. All errors reported in this paper represent one standard deviation and include both statistical and systematic errors.
18. Nearest-neighbor sites in this paper refer to the surface 1x1 lattice. The surface first and second nearest neighbors correspond to the second and third nearest neighbors in the bulk, respectively.
19. L. P. Nielson, F. Besenbacher, I. Stensgaard, E. Lægsgaard, C. Engdahl, P. Stoltze, K. W. Jacobson, and J. K. Nørskov, Phys. Rev. Lett. **71**, 754 (1993); H. Röder, R. Schuster, H. Brune, and K. Kern, Phys. Rev. Lett. **71**, 2086 (1993).
20. The temperature range during this Cr deposition was from 325 to 225 °C.
21. D. Venus and B. Heinrich, Phys. Rev. B **53**, R1733 (1996).
22. V. N. Gittsovich, V. G. Semenov, and V. M. Uzdin, J. Magn. Magn. Mater. **146**, 165 (1995).

## Figure Captions

Figure 1. STM images of Cr growth on Fe(001) at a sample bias of  $-1.1$  V. (a) Large area scan showing the layer-by-layer quality of the growth of  $0.4$  ML Cr deposited at  $290 \pm 10$  °C. (b) Small area scan of the surface shown in (a). The grey scale has been used twice through the height range of the image, each range covering approximately  $0.1$  nm. The island levels are surrounded by the thick black lines and the Fe substrate level by the thin white line. (c) Rendered perspective of the image in (b). The atomic steps are  $0.14$  nm high.

Figure 2. Tunneling conductance versus tunneling bias on the sample. The top two dashed curves are representative tunneling conductance spectra from clean Cr(001) and Fe(001) surfaces [15]. These spectra have been offset and scaled for comparison to the bottom spectra. (The scale of these spectra is lower because they were taken at a larger tip-sample separation distance.) The solid-line conductance spectra are representative of spectra taken on the submonolayer Cr/Fe(001) alloyed surface. When the tip is away from an impurity site a strong conductance peak is present at the voltage corresponding to the Fe(001) surface state. Over an impurity site the Fe(001) peak is reduced and an additional peak is present at a negative sample voltage. Both the substrate and island levels have these Fe and impurity spectroscopic characteristics, indicating that both levels are mostly Fe with a low Cr impurity concentration. A model of the Cr-Fe alloy is shown in the lower part of the figure.

Figure 3. (a) High-resolution STM image of the exposed substrate level for submonolayer Cr coverage showing the alloyed Cr impurity atoms. Simulated images of Cr pairs separated by first, second, third, and fourth nearest-neighbor (nn) distances are shown in the inset for comparison. The edges of both the real and simulated image are approximately along  $\langle 110 \rangle$  directions so the orientation of features can be directly compared. (b) Plot of the distribution of relative Cr-pair coordinates corresponding to the impurity distribution in part (a). The axes are along  $\langle 100 \rangle$  directions, which is rotated relative to the orientation in part (a). The area of each symbol is proportional to the number of Cr pairs with relative coordinates  $(x \pm \delta)_{[100]}$  and  $(y \pm \delta)_{[010]}$ , using a bin size of  $\delta = a/16$  where  $a = 0.29$  nm is the in-plane lattice constant. The scatter in the plot is due to the uncertainty ( $\pm 0.07$  nm) in identifying the relative coordinates of each impurity pair. Regions corresponding to the first, second and third nearest-neighbor separations are indicated in the figure.

Figure 4. Plot of the Cr concentration in the surface layers versus Cr deposition for the 300 °C growth condition. The empty and filled circles represent the concentrations on the substrate and the first growth layer, respectively.

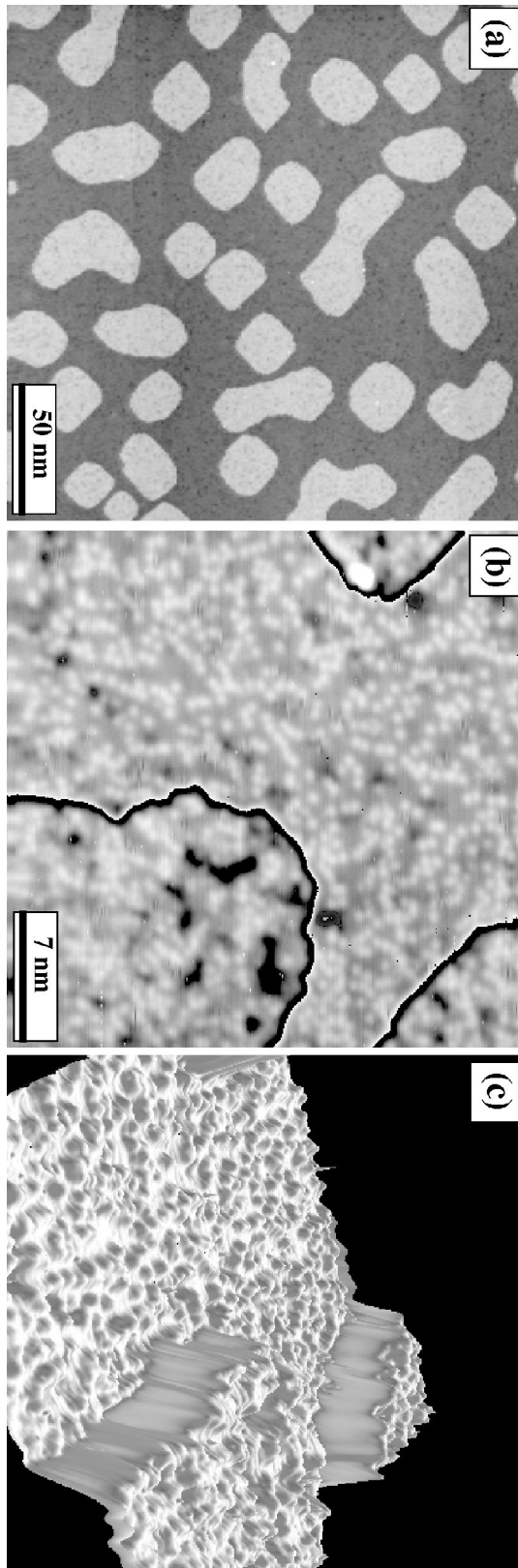


Figure 1

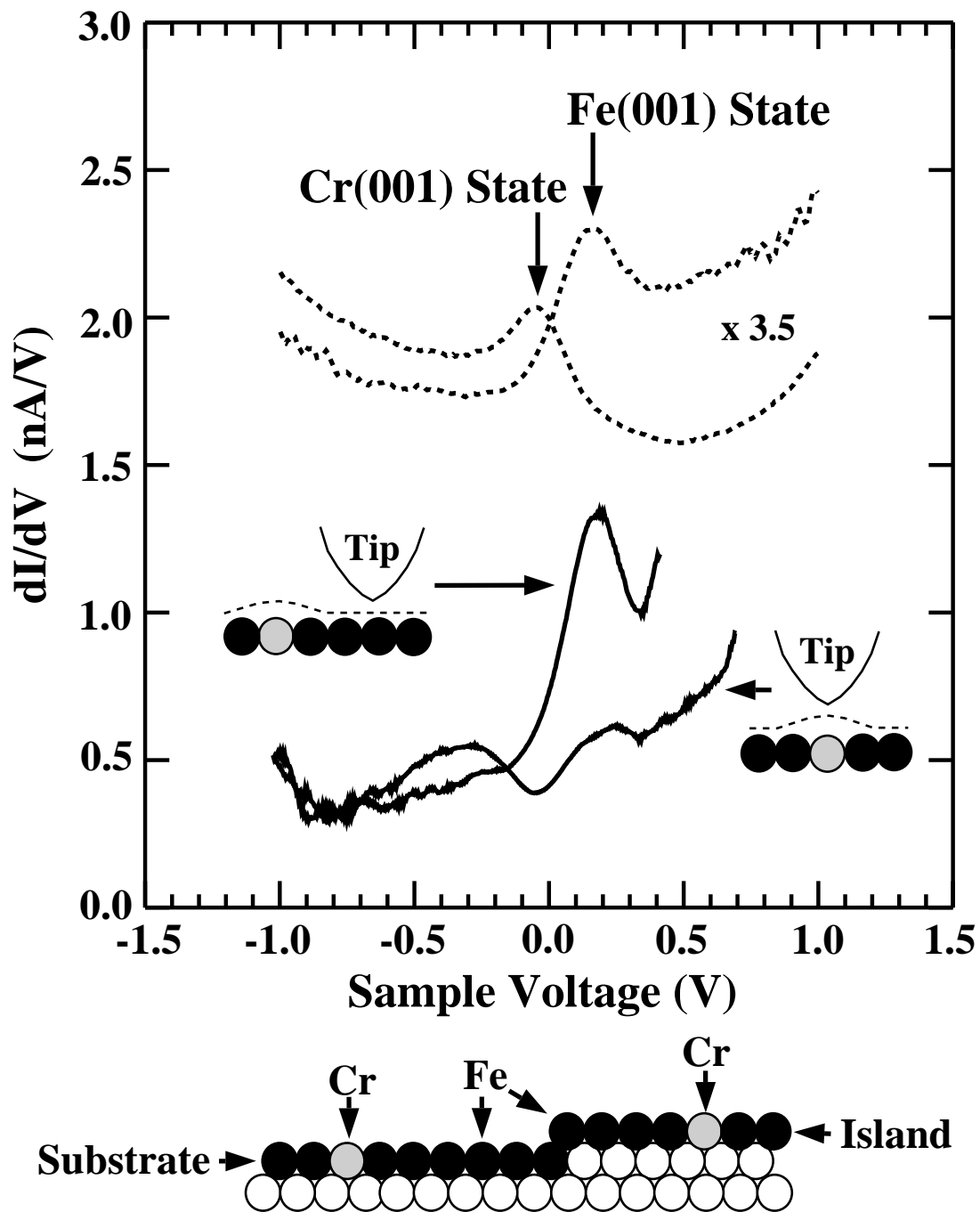


Figure 2

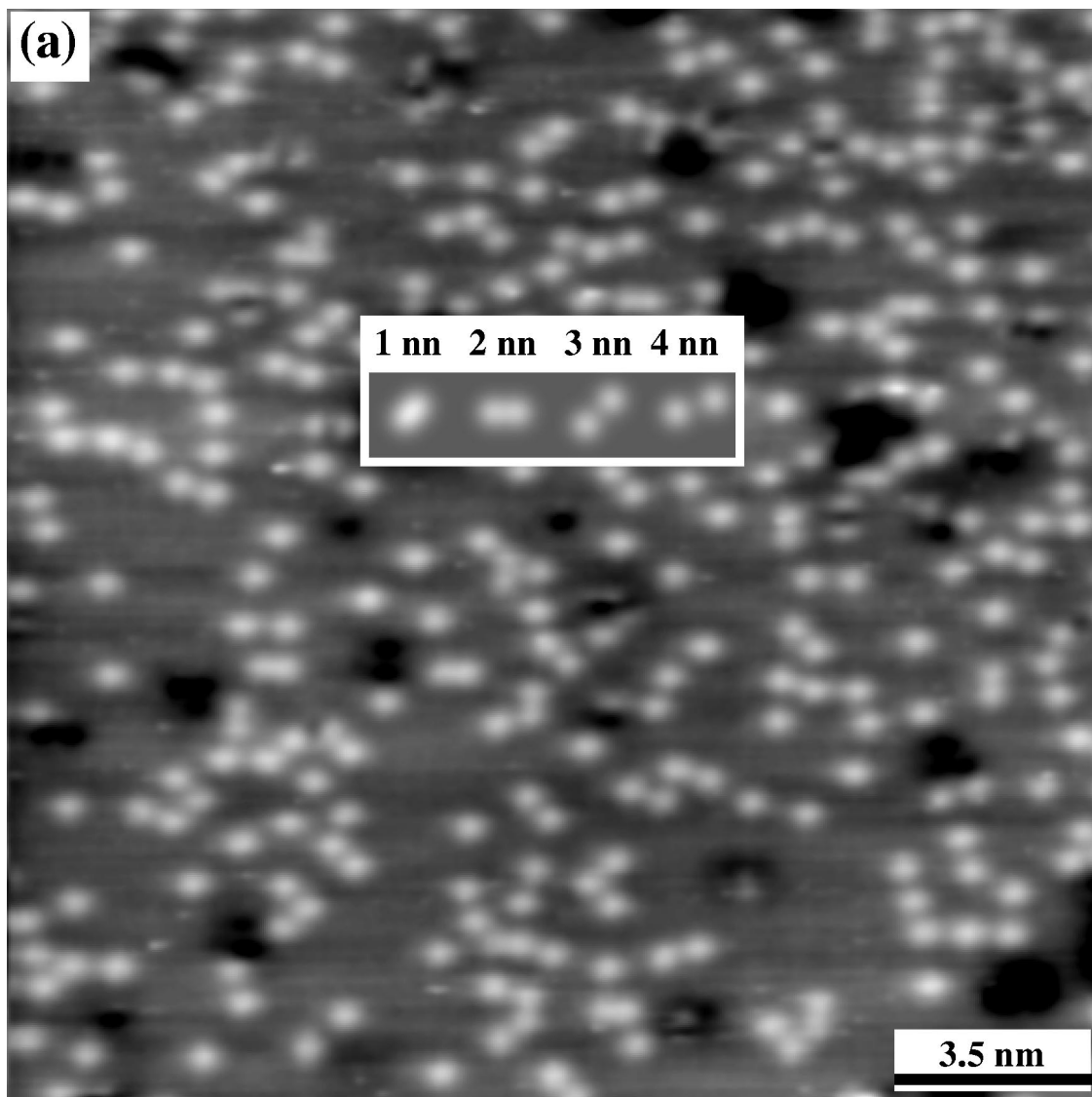


Figure 3a

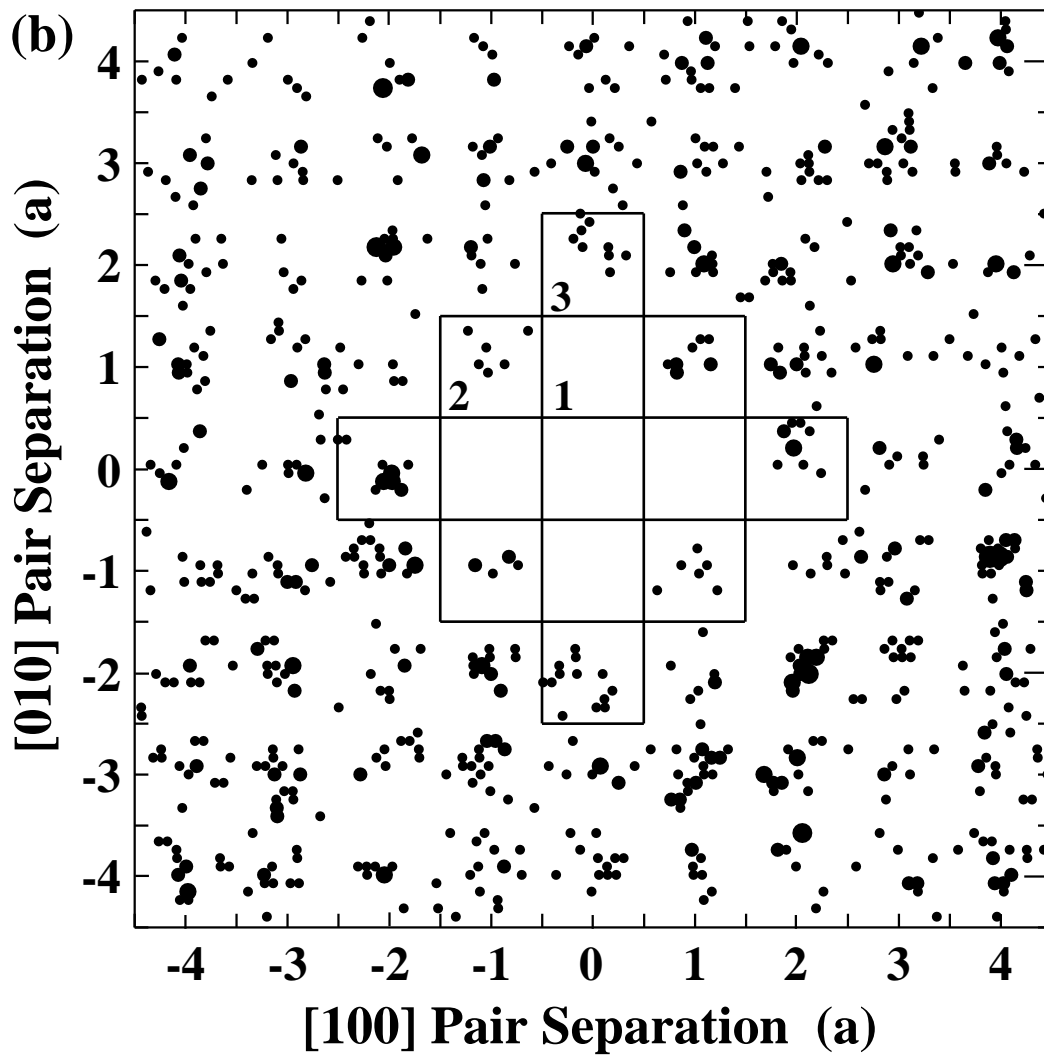


Figure 3b

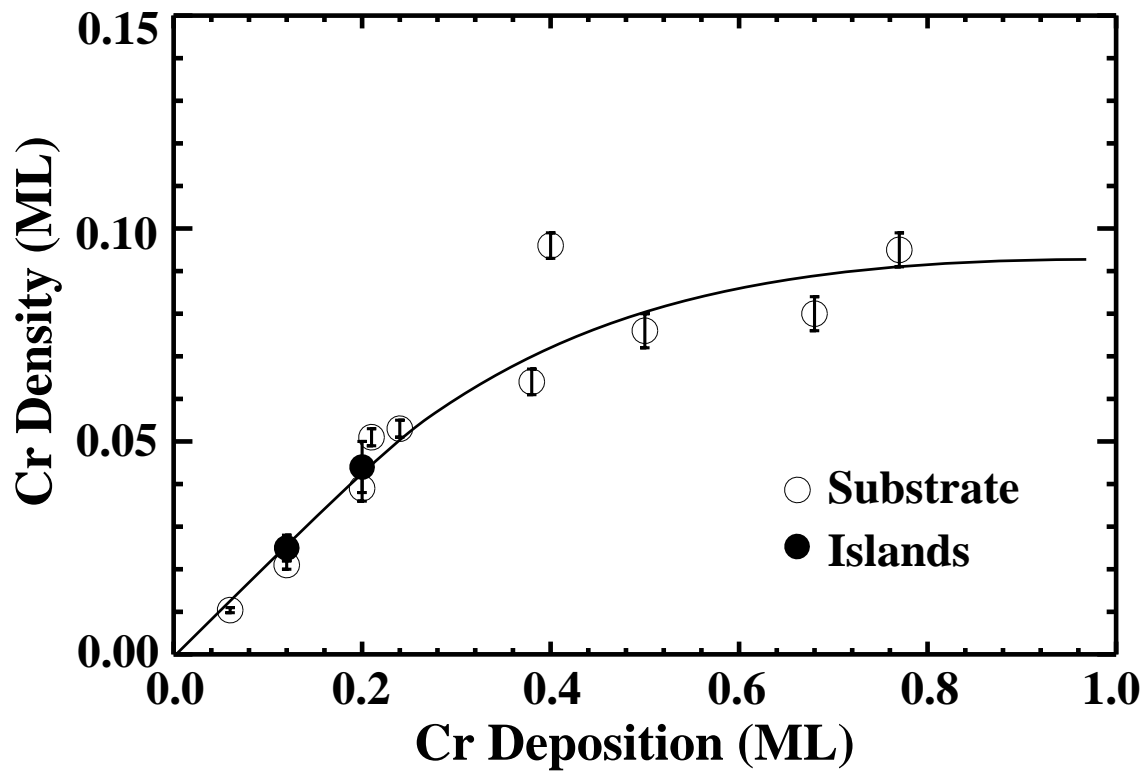


Figure 4